A copper(II) zig-zag metal–organic coordination polymer: synthesis, crystal structure, topology study, hirshfeld surface analysis and survey different conditions on morphology of a novel nano structure $[Cu(L)(SCN)(H_2O)_2]_n.2H_2O$

Bagher Souri[a], Payam Hayati[b]*, Ali Reza Rezvani[a], Rafael Mendoza-Meroño[c], and Jan Janczak[d]

[a]Department of Chemistry, Faculty of Sciences, University of Sistan and Baluchestan, Zahedan, Iran; [b]Catalan Institute of Nanoscience and Nanotechnology (ICN2), CSIC and The Barcelona Institute of Science and Technology, Barcelona, Spain; [c]Departamento de Química Física y Analítica, Universidad de Oviedo, Oviedo-CINN, Spain; [d]Institute of Low Temperature and Structure Research, Polish Academy of Sciences, Wroclaw, Poland

ABSTRACT

One copper(II) coordination polymer compound $[Cu(L)(SCN)(H_2O)_2]_n.2H_2O$ **(1)** where L stand for 2-pyridinecarboxylic acid, was synthesized following two different experimental methods, branch tube and sonochemical irradiation nano methods. Independently of the methodology used, the same crystalline phase is obtained for each compound. Single crystal X-ray analyses on compound **1** showed that Cu^{2+} ions are 6-coordinated. Additionally, H-bonds incorporate the zig-zag chains in **1** into 2D (along (1,1,0) direction) frameworks. Topological analysis shows that the compound **1** is 2C1 net. Hirshfeld surface analysis of compound **1** was studied. Also, theoretical and experimental morphology were studied. The thermal stability of compound **1** was studied by thermal gravimetric. Finally, the role of reaction time and temperature on growth and final morphology of the structures obtained by sonochemical irradiation are investigated. The results indicated that particle size was reduced with increasing sonication power, temperature, sonication time and decreasing concentration of reactant.

Introduction

The construction and designs of coordination polymer compounds (CPCs) are of current interest in the fields of supramolecular chemistry and crystal engineering.[1–3] This interest arises using their intriguing various architectures and topologies.[3–6] Furthermore, research on the synthesis and characterization of metal–organic coordination polymers is greatly motivated by their potential applications including catalysis,[3–10] gas storage,[3,5,6,8–10] magnetism,[3–7,9,10] molecular sensing,[3,6,9,10] non-linear optics,[4,5,7,10] ion-exchange,[3,4,6] electric conductivity,[4,7,9] molecular separation,[8,9] host–guest chemistry,[4,9] and medicine.[5] Therefore, rational design and synthesis of materials with specific networks has become a major research concern.[3] Numerous coordination polymers with a wide variety of structural motifs have been prepared with the variation of reagents and reaction conditions.[6,10] Copper materials are attracting an increasing number of interests due to their wildly applications in the field of catalyst, chemical sensors, luminescence, and so on.[11–18]

A number of different synthetic approaches have been offered for the preparation of coordination compounds.[19] Some of them are (1) slow diffusion of the reactants into a polymeric matrix, (2) diffusion from the gas phase, (3) evaporation from the solvent at ambient or reduced temperatures, (4) precipitation or recrystallisation from a mixture of solvents, (5) temperature controlled cooling, (6) hydrothermal synthesis, and (7) sonochemistry method.[20–24]

Sonochemistry method is easy, fast, and enables highly accurate control of synthesis parameters including time, energy input, and pH. Furthermore, the use of ultrasonic irradiation induces particle deagglomeration, which increases the surface area of the materials.[27–30] The sonochemical method enables use of the surface charge-induced hetero aggregation strategy, based on the dispersion of particles by physical methods and adjustment of the pH of the medium to a value between the points of zero charge of the materials. This maximizes the electrostatic attraction together, favoring the effective formation of heterojunctions and control of the morphology.[31–32]

Control of nano-sized building blocks therefore is essential for the future success of science and technology in the nanoscale realm.[33] With all these facts in mind the need for the development of synthetic methods in which the size and morphologies of nanostructured materials could be controlled becomes obvious both from the viewpoint of basic

sciences as well as applied technology.[35–39] The effects of ultrasound radiation on chemical reactions were reported in recent works.[40–45]

Until now, examples of $[Cu_2(L_1)(\mu\text{-}1,3\text{-}SCN)_2(SCN)]_n$ (L=4′-(4-pyridyl)-2,2′: 6′,2″-terpyridine),[46] trans-$[Cu(NCS)_2(Py)_2]$ (Py=C_5H_5N),[47] $[Cu(NCS)_2(4\text{-}MeAPy)_2]_n$ (4-MeAPy = 4-methylaminopyridine),[48] $K_2[Cu_2(sal\text{-}aa)_2(\mu\text{-}NCS)_2]n.H_2O$ (sal-aa=N-salicylideneamino acid),[49] copper(II) coordination polymer complex with different ligand are reported. However, the synthesis of lead-based 1D coordination polymers still represents a challenge. In this work, we would like to describe the rapid synthesis of nanocrystals of a copper(II) 1D CPC, $[Cu(L)(SCN)(H_2O)_2]_n.2H_2O$ (**1**), (L=2-pyridinecarboxylic acid). The power of ultrasound irradiation, sonicating time, temperature of reaction, and concentration of initial reactants were the parameters evaluated for reaching the optimized condition. Scanning electron microscopy (SEM) and powder X-ray diffraction (PXRD) were used for the characterization of the products. Additionally, we have investigated the influence of different properties (sonication power, reaction time, temperature, and concentration of reactant) on the particle morphology and size. This was achieved by using a sonochemical method.

Experimental

Materials and physical techniques

Starting reagents for the synthesis were purchased and used without any purification from industrial suppliers (Sigma-Aldrich, Merck and others). Elemental analyses (carbon, hydrogen, and nitrogen) were performed employing a Heraeus Analytical Jena, Multi EA 3100 CHNO rapid analyzer (Analytik Jena AG, Böblingen, Germany). Fourier transform infrared spectra were recorded on a FT-IR JASCO 680-PLUS spectrometer as KBr pellets in the 4000–400 cm^{-1} spectral range and Bruker Tensor 27 FT-IR with a single window reflection of diamond attenuated total reflectance (model MKII Golden Gate, Specac) and the OPUS data collection program software. The instrument is equipped with a room temperature detector, and a mid-IR source (4000–400 cm^{-1}). Since it is a single beam instrument, it was needed to run a background spectrum in air before the measurement. Single crystal X-ray diffraction experiments were carried out for compound **1** with MoKα radiation (λ=0.71073 Å) at ambient temperature. A micro focused Rigaku mm003 source with integrated confocal caxFlux double bounce optic and HPAD Pilatus 200 K detector was used for **1** while for two data were measured on a Bruker-Nonius Kappa CCD diffractometer. The structures were solved by direct methods and refined by full matrix least squares on F^2. All non-hydrogen atoms were refined anisotropically. The hydrogen atoms were included with fixed isotropic contributions at their calculated positions determined by molecular geometry, except for the oxygen bonded hydrogen atoms, which were located on a difference Fourier map and refined riding on the corresponding atoms. Computing details: data collection, cell refinement and data reduction: CrystalClear-SM expert 2.1b43[50]; program(s) used to solve structure: SHELXT[51]; program(s) used to refine structure: SHELXL-2014/7[51]; molecular graphics: PLATON[52]; reduction of data and semiempirical absorption correction: SADABS program[53]; direct methods (SIR97 program[54]); full-matrix least-squares method on F^2: SHELXL-97 program[55] with the aid of the programs WinGX[56] and Olex2.[57,58] X-ray powder diffraction (XRD) measurements were performed using an X'pert diffractometer manufactured by Philips with monochromatized Cuka radiation and simulated XRD powder patterns based on single crystal data were prepared using the Mercury software.[57] The samples were characterized with a scanning electron microscope (SEM; FEI Quanta 650 FEG) in mode operation of secondary electrons (SE) with a beam voltage between 15 and 20 KV. The samples were prepared by deposition of a drop of the material previously dispersed in properly solvents on aluminum stubs followed by evaporation of the solvent under ambient conditions. Before performing the analysis, the samples were metalized by depositing on the surface a thin platinum layer (5 nm) using a sputter coater (Leica EM ACE600). A multi wave ultrasonic generator (ultrasonic homogenizer-UP 400-A, IRAN and Elmasonic [Elma] S40 H), equipped with a converter/transducer and titanium oscillator (horn), 12.5 mm in diameter, operating at 20 kHz with a maximum power output of 400 W, were used for the ultrasonic irradiation. Melting points were measured on an electrothermal 9100 apparatus and are uncorrected.

Synthesis of $[Cu(L)(SCN)(H_2O)_2]_n.2H_2O$ (1) as single crystals

Initially, compound **1** was synthesized by the branch tube method. Branched tube equipment included on two different parts: (a) Oil bath and (b) Tube. The temperature of oil bath has been adjusted at 60 °C. It should be noted which temperature is the most important parameters in this equipment, because the difference temperature between oil bath

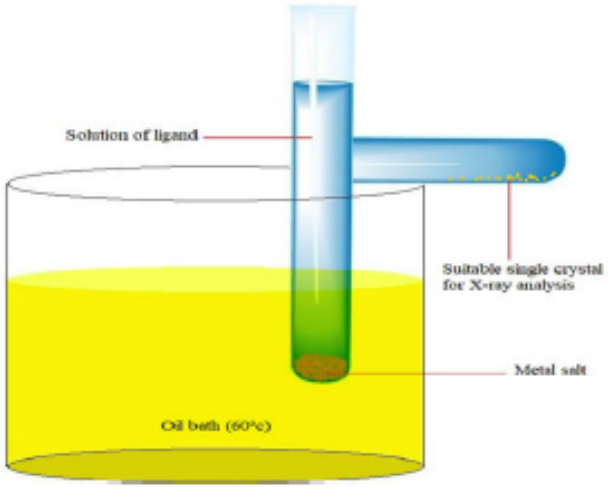

Figure 1. Depiction of the branched tube for syntheses and isolation of single crystals of the metal coordination supramolecular.

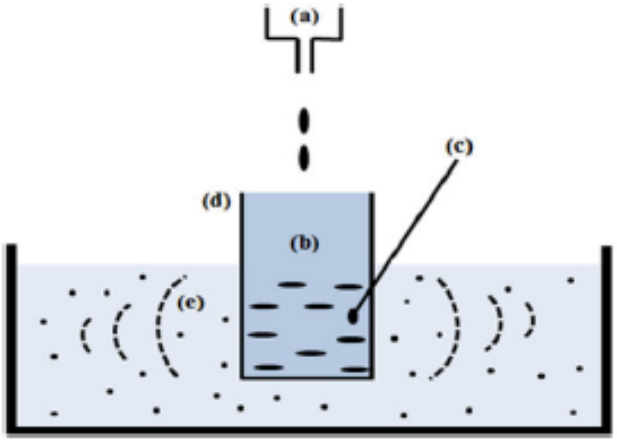

Figure 2. Schematic of the experimental setup used for the sonochemical reactions: (a) mixture of ligand and counter ion, (b) metal salt solution, (c) thermometer, (d) reaction cell, (e) ultrasound bath.

and lateral part (at room temperature) led to make convection flow. Reactants moved up to bottom in glass, spontaneously. In fact convection flow has role of the stirrer. Quality crystals were synthesized by this method after one week. An important advantage of this method in comparison with other crystallization methods which is reactant materials are placed in the bottom of the solvent without dissolving and they react slowly and finally good crystals were obtained (Figure 1).

$Cu(NO_3)_2.2.5H_2O$ (1 mmol, 0.232 g), 2-pyridinecarboxylic acid (L) (1 mmol, 0.246 g) and KSCN (2 mmol, 0.18 g) were loaded into one arm of a branch tube and both of the arms were filled slowly with water. The chemical bearing arm was immersed in an oil bath kept at 60 °C. Crystals were formed on the inside surface of the arm kept at ambient temperature. After 5 days, colorless crystals were deposited in the cooler arm. The crystals obtained were filtered off, washed with water and air dried. (0.124 g, 39.36% yield based on final product), product **1** (single crystal): m.p > 300 °C. Anal. Calc. for $C_7CuH_{12}N_2O_6S$: C: 26.59%, H: 3.79%, N: 8.87%, O: 30.39%; Found C: 26.51%, H: 3.28%, N: 8.86%. IR (selected bands for compound **1**; in cm^{-1}): 3441(b), 3075(w), 1647(s), 1605(s), 1349(s), 776(s) cm^{-1}.

Synthesis of $[Cu(L)(SCN)(H_2O)_2]_n.2H_2O$ (1) under ultrasonic irradiation

The study of sonochemistry is concerned with understanding the effect of ultrasound in forming acoustic cavitation in liquids, resulting in the initiation or enhancement of the chemical activity in the solution. Therefore, the chemical effects of ultrasound do not come from a direct interaction of the ultrasonic sound wave with the molecules in the solution. The simplest explanation for this is that sound waves propagating through a liquid at ultrasonic frequencies do so with a wavelength that is significantly longer than that of the bond length between atoms in the molecule. Therefore, the sound wave cannot affect that vibrational energy of the bond, and can therefore not directly increase the internal energy of a molecule. Instead, sonochemistry arises from

Table 1. Crystal data and structures refinement for $[Cu(L)(SCN)(H_2O)_2]_n.2H_2O$ (1).[74]

Empirical formula	$C_7H_8CuN_2O_4S\cdot 2(H_2O)$
Formula weigh	315.79 g/mol
Temperature	100 K
Wavelength	0.71073 Å
Crystal system	Orthorhombic
Space group	Pbca
Unit cell dimensions	$a = 8.6480$ (1)Å, $\alpha = 90°$ $b = 10.6260$ (2)Å, $\beta = 90°$ $c = 26.2969$ (6)Å, $\gamma = 90°$
Volume	2416.52 (8)$Å^3$
Z	8
Crystal size	0.33 × 0.27 × 0.21 (mm)
Absorption coefficient	19.068 Mg/m^3
$F(0\ 0\ 0)$	1288
Theta range for data collection	2.8°–29.6°
μ	2 mm^{-1}
Index ranges	$-11 \leq h \leq 11$ $-13 \leq k \leq 13$ $-36 \leq l \leq 34$
$(\sin\theta/\lambda)$max	0.694$Å^{-1}$
Theta (max)	29.6°
Radiation type	Mo Kα
Refinement method	Full-matrix least-squares on F^2
Goodness-of-fit on F^2	1.041
Refinement	$R[F^2 > 2\sigma(F^2)] = 0.025$ $wR(F^2) = 0.064$ $S = 1.00$
R1 [I > 2σ(I)]	25166, 3122, 2818
Rint	0.026
Largest diff. peak and hole	−0.37 and 0.35 eA^{-3}
CCDC no.	1552099

Table 2. Selected bond lengths/A° for compound $[Cu(L)(SCN)(H_2O)_2]_n.2H_2O$ (1).[74]

Cu(1)—N(1)	1.9480(14)	O(3)—H(31)	0.847(5)
Cu(1)—O(1)	1.9612(11)	O(3)—H(32)	0.848(5)
Cu(1)—O(3)	1.9675(11)	O(4)—H(41)	0.849(5)
Cu(1)—N(2)	1.9989(14)	O(4)—H(42)	0.849(5)
Cu(1)—S(1)	2.882(6)	O(5)—H(51)	0.847(5)
C(1)—S(1)	1.6375(16)	O(5)—H(52)	0.847(5)
N(2)—C(2)	1.338(2)	O(6)—H(61)	0.847(5)
N(2)—C(6)	1.352(2)	O(6)—H(62)	0.847(5)

Symmetry code: [a]1/2−x, −1+2+y, z; [b] 1/2−x, 1+2+y, z; −. [c]1/2 −x, 1 1 2+y, z; [d]1/2 + x, 1/2 −y, −z.

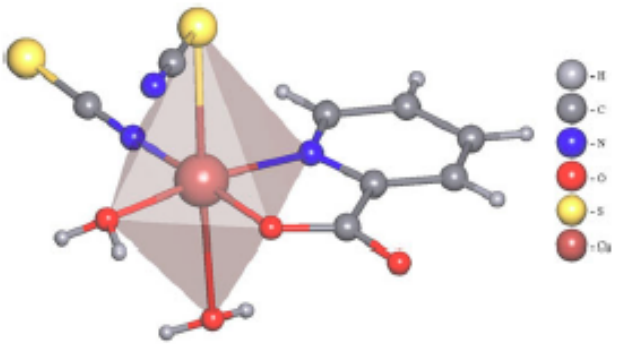

Figure 3. Coordination around Cu^{+2} cations in $[Cu(L)(SCN)(H_2O)_2]_n.2H_2O$ (1).

acoustic cavitation: the formation, growth, and implosive collapse of bubbles in a liquid. The collapse of these bubbles is an almost adiabatic process, thereby resulting in the massive build-up of energy inside the bubble, resulting in extremely high temperatures and pressures in a microscopic region of the sonicated liquid. The high temperatures and pressures result in the chemical excitation of any matter that was inside of, or in the immediate surroundings of the

bubble as it rapidly imploded. A broad variety of outcomes can result from acoustic cavitation, including sonoluminescence, increased chemical activity in the solution due to the formation of primary and secondary radical reactions, and increase chemical activity through the formation of new, relatively stable chemical species that can diffuse further into the solution to create chemical effects (e.g. the formation of hydrogen peroxide from the combination of two hydroxyl radicals formed following the dissociation of water vapor inside the collapsing bubbles what water is exposed to ultrasound (Figure 2). In generally, sonochemistry method is fast method in compared to solvothermal, hydrothermal, branched tube, solvent diffusion, etc methods.[59,60]

Three nanostructures of $[Cu(L)(SCN)(H_2O)_2]_n.2H_2O$ (**1**) were prepared by sonochemical process. Firstly, a high-density ultrasonic probe was immersed directly into the solution of $Cu(NO_3)_2.2.5H_2O$ (10 ml, 0.05 M) in water. Then into this solution, a proper volume of KSCN (10 ml, 0.05 M) and 2-pyridinecarboxylic acid (L) (10 ml, 0.05 M) ligand in water solvent was added in a drop wise manner. The solution was irradiated by ultrasound at 60 W and temperature 30 °C. After 30 min, a white powder was obtained (temperature: 30 °C reaction time: 30 min, sonication power: 60 W, concentration: 0.05 M). Following the above process, the role of temperature and time reaction was studied. Firstly, for the study of the effect related with the temperature, the reaction described was carried out at 60 °C (reaction time: 30 min, sonication power: 60 W, concentration: 0.05 M). The reaction time was increased up to 60 min (temperature: 30 °C, sonication power: 60 W, concentration: 0.05 M). Finally, the concentration of reactants was investigated to 0.1 M (temperature: 30 °C, sonication power: 60 W, reaction time: 30 min). In all the cases, the obtained precipitates were filtered, subsequently washed with water and then dried.

Compound **1**: (0.162 g, 51.42% yield based on final product), product **1**: m.p > 300 °C. Anal. Calc. for $C_7CuH_{12}N_2O_8S$: C: 26.59%, H: 3.79%, N: 8.87%, O: 30.39%; Found C: 26.54%, H: 3.54%, N: 8.73%, O: 30.32%. IR

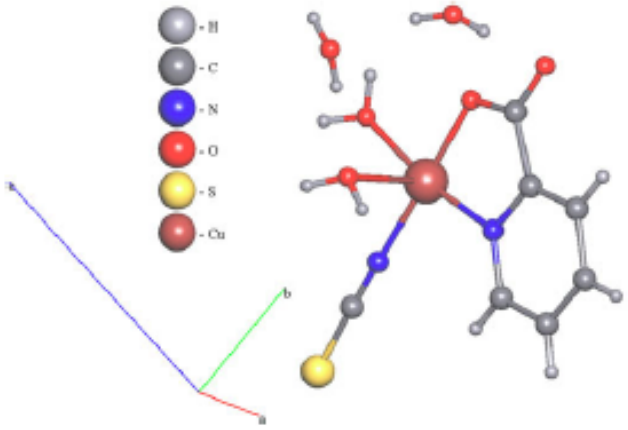

Figure 4. Asymmetric unit of compound of $[Cu(L)(SCN)(H_2O)_2]_n.2H_2O$ (1).

Table 3. Selected bond lengths (Å) and angles (°) in copper(I), (II) coordination compounds.

Compounds	Cu–N	Cu–S	Ref.
$[Cu(L)(SCN)(H_2O)_2]_n.2H_2O$	1.948(14)	2.882(6)	This work
$[Cu(I\text{-}N,SNCS)_2(isn)_2]n$	1.950(1)	2.949(4)	[75]
$[\{(Cu_2L_2)\}\{CuI_4(\mu\text{-}1,3\text{-}SCN)_2(\mu\text{-}1,1,3\text{-}SCN)_4\}]_n$	2.007(2)	2.713(2)	[76]
$[\{(Cu_2L_2)\}\{Cu_2(\mu\text{-}1,3\text{-}SCN)_2(\mu 1,1,3\text{-}SCN)_2\}]_n$	2.020(3)	2.720(1)	[76]
$[Cu(4\text{-}Bipy)_2(NCS)_2]$	1.958(8)	3.078(10)	[77]
$[Cu(4\text{-}pic)_2(NCS)_2]$	2.003(8)	3.109(4)	[78]
cis-$[Cu(SCN)_2(bopy)_2]$	2.009(4)	–	[79]
trans–$[Cu(SCN)_2(bopy)_2]$	1.965(14)	–	[79]
$[CuCl_2(bopy)_2]$	2.006(17)	–	[79]
$[Cu(NCS)_2(pyrimidine)_2]_n$	2.040(2)	2.808(10)	[80]
$[Cu(SCN)(3\text{-}Acpy)_2]_n$	2.072(5)	2.479(7)	[81]
$[Cu_2(SCN)_4(3\text{-}Acpy)_4]$	2.048(2)	2.863(1)	[81]
$[Cu_2(\mu\text{-}dea)_2(NCS)_2]$	1.926(17)	–	[82]
$[Cu_2(taec)(NCS)_2](ClO_4)_2\cdot H_2O$	2.085(5)	–	[83]
$[Cu(4\text{-}cpy)(SCN)_2]_n$	2.023(2)	2.867(1)	[84]
$[Cu(2\text{-}ambzim)(SCN)_2]_n$	1.975(3)	2.952(13)	[84]
$[Cu_2(\mu\text{-}SCN)_2(SCN)_2(pybzim)_2]$	1.970(2)	2.942(8)	[84]
$[Cu(SCN)_2\{(py)_2C(OEt)(OH)\}]_2.2EtOH$	2.033(16)	2.925(9)	[85]

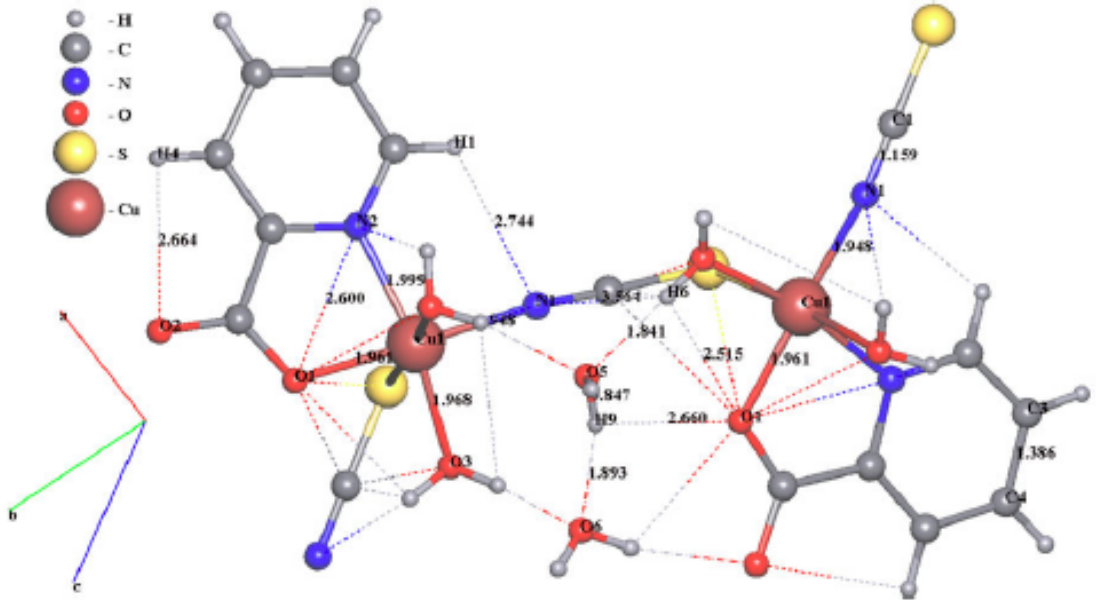

Figure 5. Selected distances for compound $[Cu(L)(SCN)(H_2O)_2]_n.2H_2O$ (1).

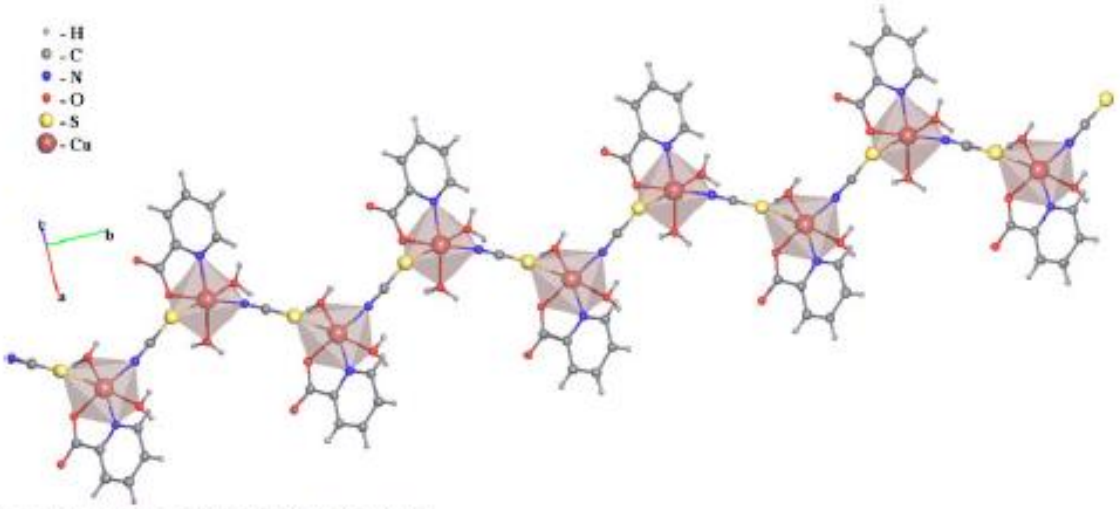

Figure 6. Zig-zag chains of 1 D in CPC $[Cu(L)(SCN)(H_2O)]_n.2H_2O$ 1.

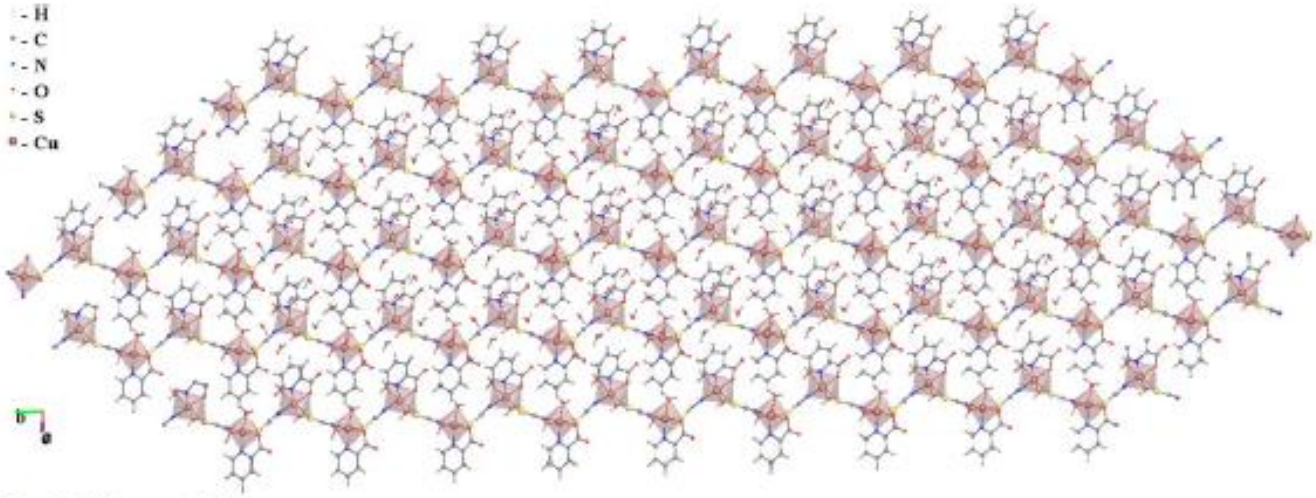

Figure 7. 2D fragments of 1.

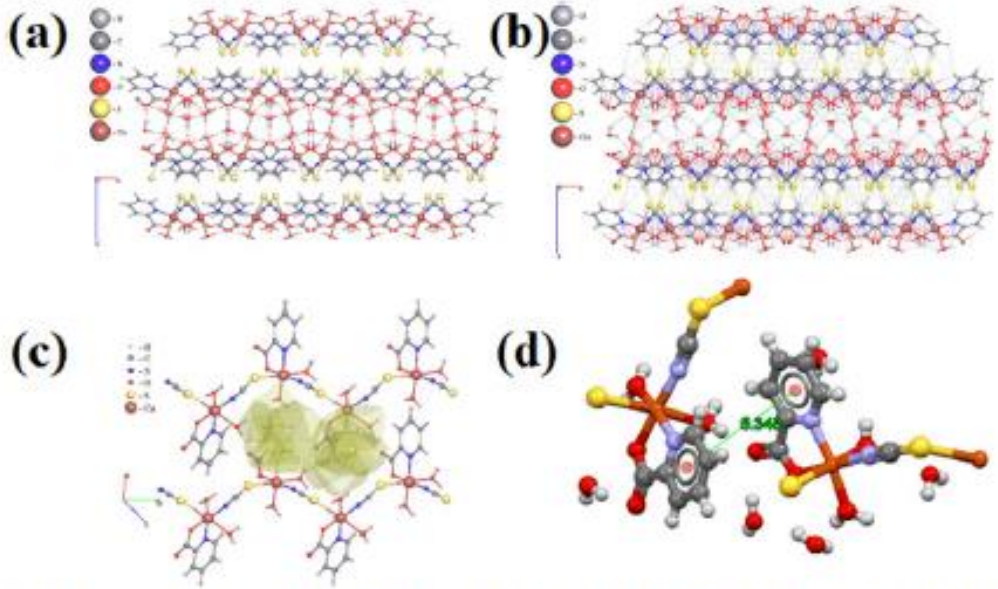

Figure 8. Interactions within molecules of $[Cu(L)(SCN)(H_2O)]_n.2H_2O$ 1: (a) Hydrogen bound interaction, (b) van der Waals interaction, (c) π−π interaction and (d) distance of aromatic rings (bottom).

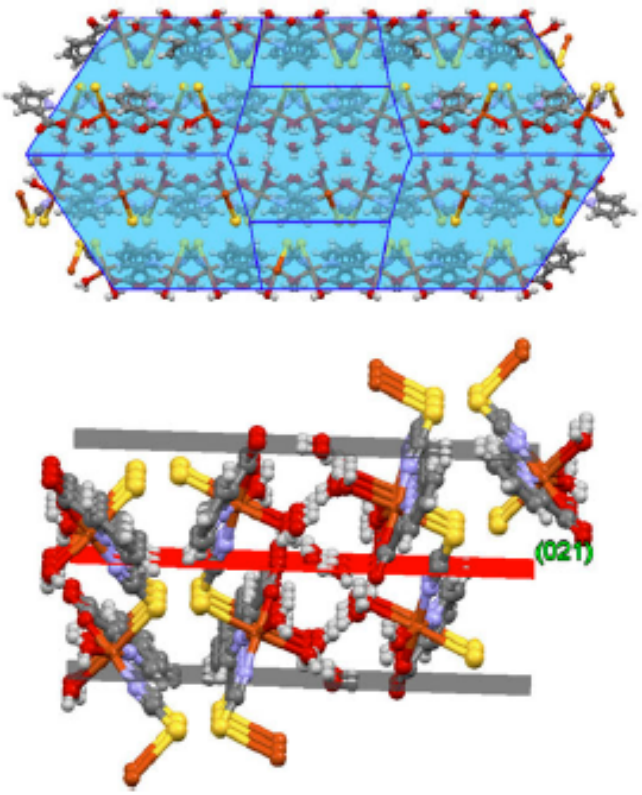

Figure 9. Predicted crystal morphologies of $[Cu(L)(SCN)(H_2O)_2]_n.2H_2O$ **1** (up) and their packing along the [010] for $[Cu(L)(SCN)(H_2O)_2]_n.2H_2O$ **1** (down).

(selected bands for compound **1**; in cm^{-1}: 3440(b), 3079(w), 1647(s), 1605(s), 1348(s), 778(s) cm^{-1}.

Results and discussion

Initially, compound **1** was synthesized by the branch tube method. For the synthesis of compound **1**, $Cu(NO_3)_2.2.5H_2O$, 2-pyridinecarboxylic acid (**L**) and KSCN were loaded into one arm of a branch tube while filling both arms slowly with water. The chemical bearing arm was afterwards immersed in an oil bath kept at 60 °C while the second remains at room temperature. After 5 days, colorless crystals were deposited in the cooler arm. The crystals obtained were filtered off, washed with water, air dried and finally characterized as compound **1** (vide infra).

X-ray characterization

Selected crystals of compound **1** was isolated and analyzed by X-ray diffraction, crystallizing both in an orthorhombic Pbca space group. For more crystallographic details see Tables 1 and 2.

Compound 1. The Pb atoms of **1** are coordinated by two N atoms, three O atoms and one S atom composing octahedral coordination O_3N_2S (Figure 3). The asymmetric unit of compound **1** contain one Cu^{2+} cation, which is coordinated to one 2-pyridinecarboxylic acid ligand ($L=C_6H_5NO_2$), one SCN^- anions and two H_2O molecules which are in crystal lattice (Figure 4). Each 2-pyridinecarboxylic acid ligand ($L=C_6H_5NO_2$) in compound **1** is coordinated to one Cu atom by one N atom of pyridine ring (Cu–N distance: 2.343 Å) and one O atoms of carboxylic acid group (Cu–O distance: 1.96 Å). Additionally, one bridge SCN atoms are coordinated to two Cu atoms through Cu(1)–N1 and Cu(1)–S1 bounds (Cu–N and Cu–S distances are 1.948 and 2.882 Å, respectively; Table 2 and Figure 5). The length of Cu–N and Cu–S bonds are shown for some of coordination supramolecular compounds based on copper metal in Table 3. It should be noted that the coordination interactions can be separated in two groups: strong (more valence, in short range 0.845–2.520 Å) and weak (more electrostatic, in long range 2.664–3.570 Å). Strong bonds form mononuclear compounds $[Cu(L)(SCN)(H_2O)_2]$, which expanded by relatively weak interactions in polymeric layer $[Cu(L)(SCN)(H_2O)_2].2H_2O$. Also structures of compound **1** are two-periodic ([1,1,0] orientation) and one-periodic (in [0,1,0] direction) coordination polymer architectures (Figures 6 and 7). Each isothiocyanate groups is linking two similar copper atoms. These 1D zig-zag chains are bridged by the isothiocyanate groups through forming and expanded by hydrogen bound, π–π stacking and van der Waals interactions a layer on the *ab* crystal plane (Figures 6, 8, and 9). It should be noted that additional weak π–π interaction reinforces CPC. The π–π interactions in **1**, are due to the presence of the rings of pyridine (distance of two pyridine rings: 5.348 Å) allowing the interactions between the parallel chains (Figures 8 and 9).

The morphology and size of products prepared by the sonochemical method were examined by SEM, (Figure 10). The SEM micrographs of compound **1** show plate morphology. Bravais Friedel Donnay Harker (BFDH) analysis was carried out in order to estimate the faces that are supposed to appear in the crystals morphology (Figure 9). This analysis considers the effect of symmetry operations on the interplanar distances of crystal faces.[63] Predicted crystal morphologies of compound **1** are shown in Figure 11. In almost all cases there is a good match between the predicted and observed morphology. It should be noted that in the case of **1**, the growth of the coordination material takes place along the [021] directions (Figure 9).

Each $[Cu(L)(SCN)(H_2O)_2]_n.2H_2O$ chain is located between six other same chains forming van-der-Waals, hydrogen bonded and π–π interactions hexagonal packing, which corresponds to geometrically octahedral packing (Figures 9 and 12). Simplification of the chain to the underlying net by ToposPro package reveals 2C1 topological type (Figure 13), which is abundant for 1D coordination polymers (56,607 examples in TTO collection of ToposePro).[61,62]

Hirshfeld surface analysis

The crystal structure from the title compound as discussed below is a good example of the interplay of different molecular interactions. In order to analyses the various interactions that lead to the crystal structure, an intermolecular intercontacts leading to the Hirshfeld surfaces has

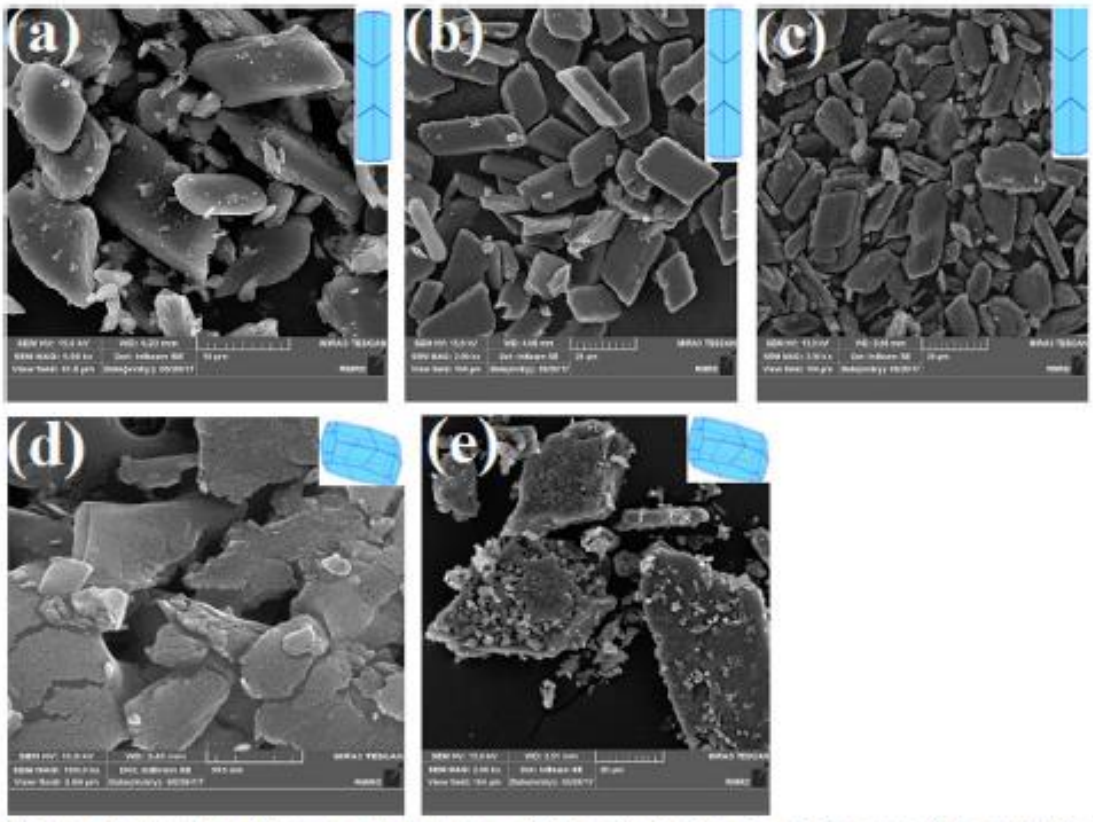

Figure 10. SEM images of compound **1**, (a) Compound **1-1** (temperature: 30 °C, reaction time: 30 min, sonication power: 0 W, concentration: 0.05 M); (b) Compounds **1** and **2** (temperature: 30 °C reaction time: 30 min, sonication power: 60 W, concentration: 0.05 M); (c) Compounds **1–3** (temperature: 30 °C reaction time: 60 min, sonication power: 60 W, concentration: 0.05 M); (d) Compounds **1–4** (temperature: 60 °C, reaction time: 30 min, sonication power: 60 W, concentration: 0.05 M), (e) (d) Compounds **1–5** (temperature: 30 °C, reaction time: 30 min, sonication power: 60 W, concentration: 0.1 M).

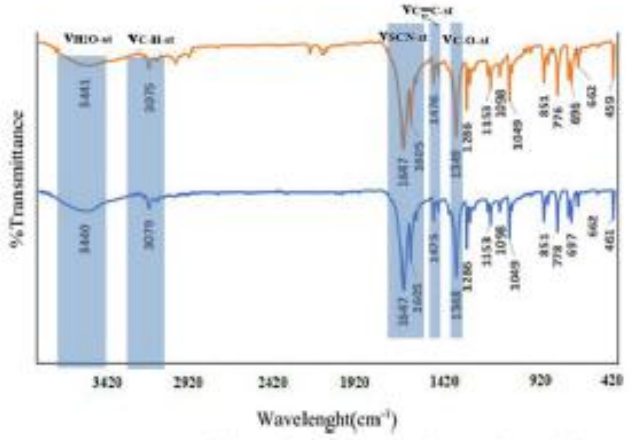

Figure 11. FT-IR spectra of (brown line) bulk materials as synthesized of compound **1** and (blue line) nano-sized compound **1** prepared by sonochemical method.

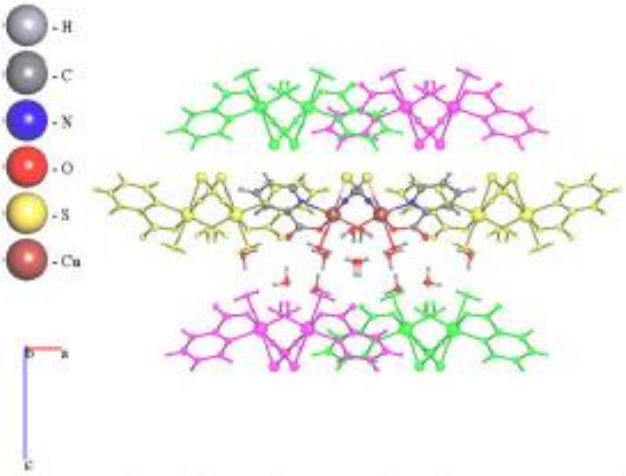

Figure 12. Number of chains, chains surrounding the constitutive unit of $[Cu(L)(SCN)(H_2O)_2]_n{\cdot}2H_2O$ **1**.

been made. The Hirshfeld surface considered the volume of space where molecule electron density exceeds that all neighboring molecules.[64,65] Molecular Hirshfeld surfaces have been constructed from CIF file, so that you can dissect crystal structures into noncovalent contacts The very high-resolution Hirshfeld surfaces were generated by Crystal Explorer and functions of curvature, distance including shape index and dnorm were mapped to the surfaces.[66–71] The function dnorm is a normalized distance property defined with regards to d_i (distance from a point on the Hirshfeld surface to the nearest internal nucleus), d_e (distance from a point on the Hirshfeld surface to the nearest external nucleus) and van der Waals radii (r_i^{dvW} and r_e^{dvW}): $d_{norm} = [(d_i - r_i^{dvW})/r_i^{dvW}] + [(d_e - r_e^{dvW})/r_e^{dvW}]$.[22–24] Thus, the value of d_{norm} was negative or positive when intermolecular contacts were shorter or longer than r^{vdW}, respectively. The Hirshfeld surfaces of the title compound

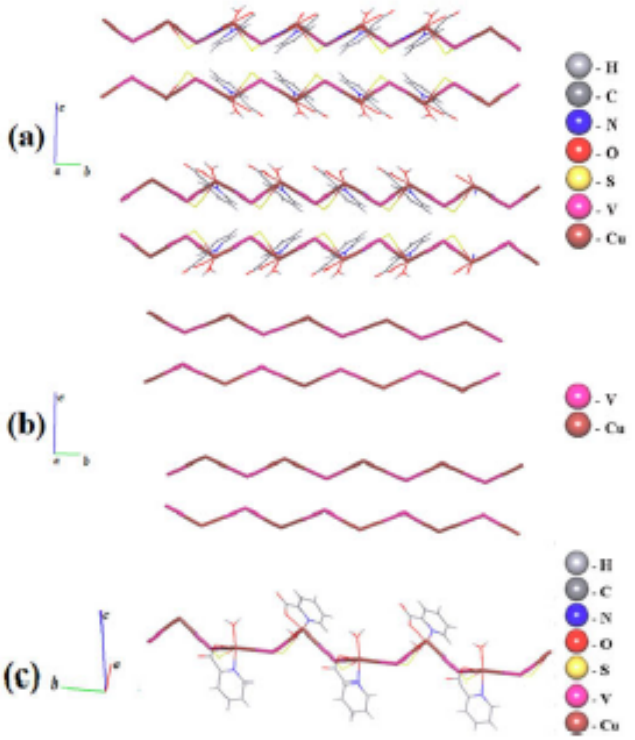

Figure 13. (a): The 1D chain of **1** is formed by Cu(II), L and SCN\bar along crystallographic '*b*' axis. (b): Simplified network of **1**. (c): The building blocks of network **1**.

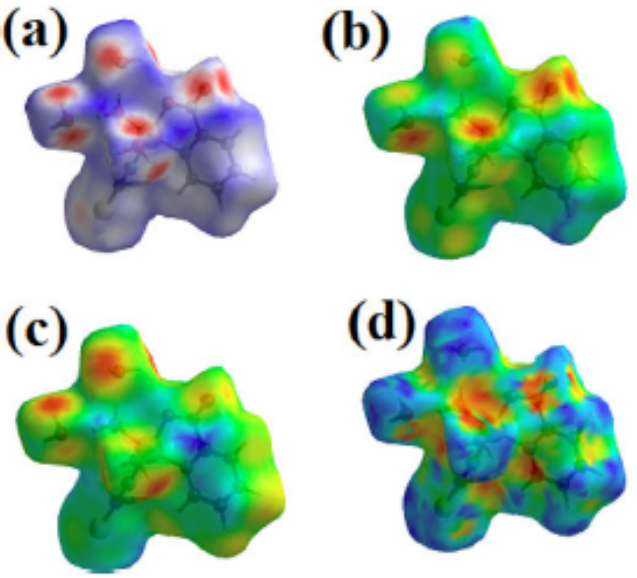

Figure 14. Hirshfeld surface analysis of **1**: (a) d_{norm}, (b) d_e, (c) d_i, (d) shape-index.

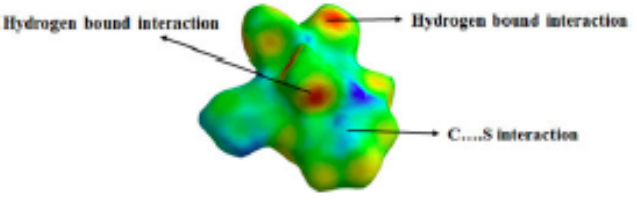

Figure 15. Hirshfeld surfaces of **1** surface index.

(Figure 14) were mapped over a d_{norm}, d_e, d_i, curvedness, and shape-index.

The d_{norm} values were mapped to the Hirshfeld surface (Figure 14(a)) by using a red–blue–white color scheme as follows: red regions represented closer contacts as well as a negative dnorm value; blue regions represented longer contacts and a positive dnorm value; and white regions represented the distance of contacts equal to precisely the van der Waals separation with a d_{norm} value of zero. These normalized contact distances (d_{norm}) reveal the close contacts of hydrogen bond donors and acceptors, but other close contacts are evident. Actually, Figure 12(a) reveals that the large circular depressions are the indicators of hydrogen bonding contacts and the dominant interactions are O–H whereas other visible spots are due to H–H contacts, based on both d_e and d_i. Particularly, adjacent red/orange and blue triangle like patches on a shape index map (Figure 15) give us information about hydrogen bound and C…S interaction.[66,69–73] The combination of the distances from the Hirshfeld surface to the nearest nucleus inside the surface (d_i) and outside the surface (d_e) and the data conveyed by the shape index are consistent with 2D fingerprint plots.[64,65]

The 2D fingerprint maps of **1** provide some quantitative information gives the possibility of obtaining additional insight to the intermolecular interactions in the crystal state and for describing the surface characteristics of the molecules (Figure 16). Globally, H… …H, H… …O, C… …H, and S….H intermolecular interactions were most abundant in the crystal packing (29.8%, 24.6%, 14.1%, and 11.4%, respectively). It really is evident that van der Waals forces exert an important influence on the stabilization of the packing in the crystal structure, and other intercontacts [N… …H/H… ….N (4.0%), C….O (4.0%), C… …S (3.7%), N… …S (2.5%), and H… …Cu (0.1%)] contribute less to the Hirshfeld surfaces. On the other hand, the relative contributions of the different interactions to the Hirshfeld Surfaces were also calculated for the title compound (Figure 17 and Table 4).

Sonochemical synthesis

Synthesis of compound **1** was alternatively achieved by the application of ultrasounds. For the synthesis of compound **1**, a high-density ultrasonic probe was immersed directly into a water solution $Cu(NO_3)_2 2.5H_2O$ and posterior drop wise addition a second water solution of KSCN and 2-pyridinecarboxylic acid (**L**). The synthesis were done the reactants concentration and the ultrasound power while other factors such as temperature and the reaction time were systematically modified (a resume of the different reactions is shown in Table 5).

PXRD of compounds is similar to that obtained upon simulation from the X-ray diffraction data obtained for **1**. As Figure 18 reveals that both (experimental and simulation) exhibit the same crystalline phase. These results indicate the existence of a single crystalline phase, which is maintained independently of the synthesis method (Figure 10).

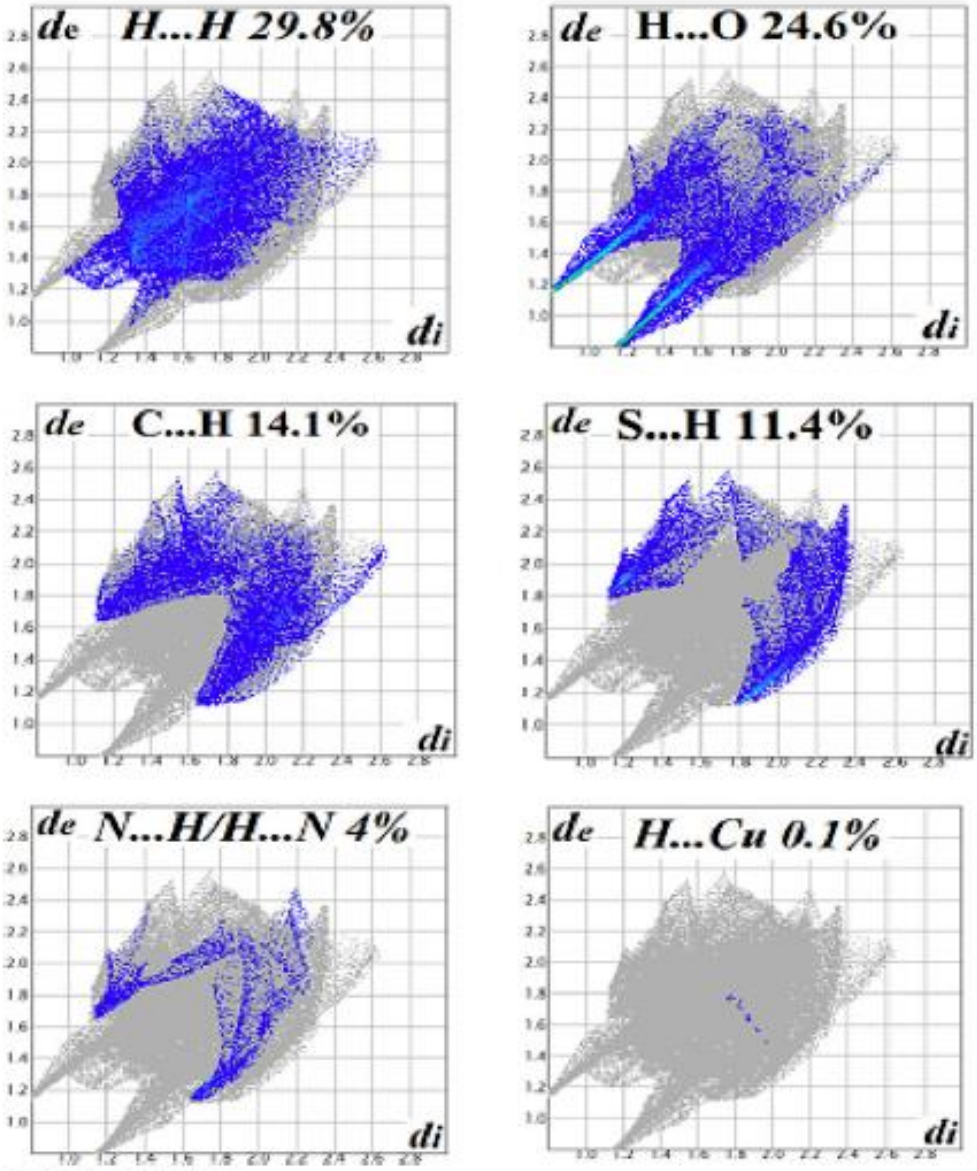

Figure 16. Fingerprint plots of major contacts in 1.

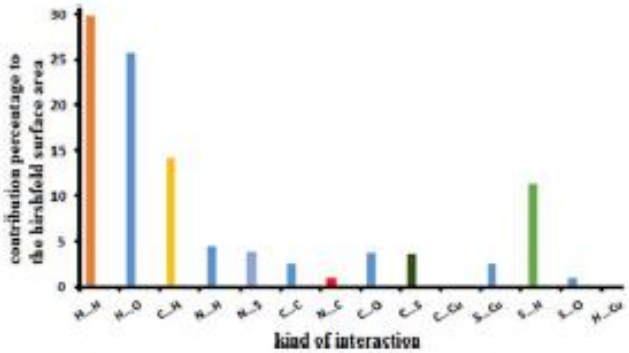

Figure 17. The relative contributions to the Hirshfeld surface area for 1.

Various conditions for preparation of compounds **1** nano-structure were summarized in Table 5. In this table, sample 1–1, were studied without power ultrasound and the other samples were studied under variable temperature, time and power ultrasound. In order to research the role of power ultrasound irradiation on the character of product, reactions were performed under completely different power ultrasound irradiation. Results show a decrease in the particles size as increasing power ultrasound irradiation. In sample 1–1, the reactions were studied without power ultrasound. Results show that size particles sample of 1–1 (Figure 10(a)) is larger than 1–2 (Figure 10(b)). Table 5 shows the average diameter scanning electron micrographs (SEM) of the prepared samples. Results show high power ultrasound irradiation decreased agglomeration, and thus led to decrease particles size. Comparison between samples 1–2 and 1–3 shows a decrease in nanoparticle size. Thus, size particles of sample 1–3 are smaller than 1–2 (Figure 10(c)). However, a reducing the reaction time led to the decrease of size particles of sample 1–3. Particle sizes and morphology of nanoparticle are depending on temperature. Higher temperature (60 °C) results in an increased solubility, and thus

Table 4. Contribution to hirshfeld surface area of different interaction in compounds 1.

Interactions	Contribution to hirshfeld surface area (%)	Interactions	Contribution to hirshfeld surface area (%)
Cu....C	0.1	N....S	2.5
Cu....S	2.6	S....S	3.7
Cu....H	0.1	S....O	0.9
C....Cu	0.1	H....Cu	0.1
C....C	1.1	H....N	4.1
C....S	3.7	H....C	14.1
C....H	14.1	H....S	11.4
C....O	4.0	H....H	29.8
H....N	4.0	H....O	24.6
H....C	14.1	H....Cu	0.1

Table 5. The influence of ultrasound power, reaction time, temperature and concentration of reactants on the morphology of compounds 1 particle.

Compound 1	M(mol/l)[a]	T (°C)[b]	T (min)[c]	Sonication (W)	SEM[d]	Morphology
1–1	0.05	30	30	0	548	Mix morphology
1–2	0.05	30	30	60	183	Nano plate
1–3	0.05	30	60	60	92	Macro plate
1–4	0.05	60	30	60	168	Macro plate
1–5	0.1	30	30	60	378	Mix morphology

[a]Concentration of initial reactant.
[b]Reaction temperature.
[c]Reaction time.
[d]Average diameter.

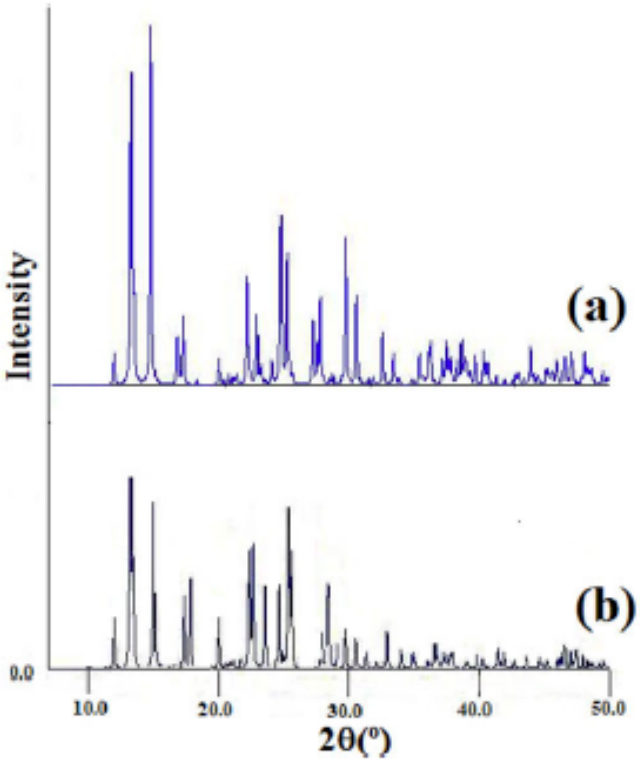

Figure 18. (a) PXRD patterns corresponding to the simulation of single crystal X-ray data compound 1 and (b) corresponding to the nano-structured systems 1.

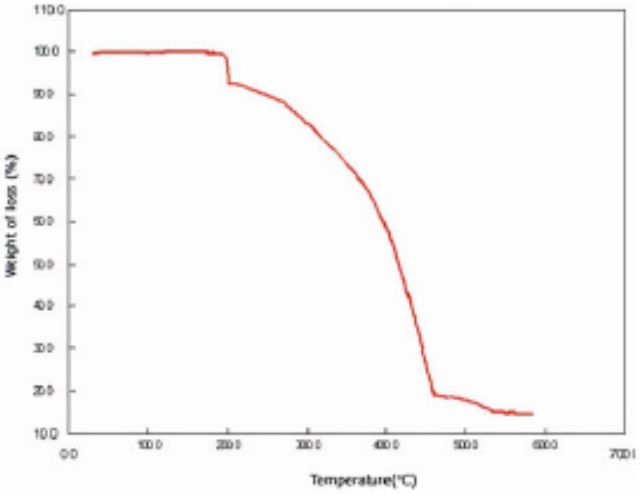

Figure 19. Thermal behavior of compound 1.

a reduced supersaturation of growth species in the solution, and thus particles size of sample 1–4 is smaller than particles size of sample 1–2 (Figure 10(b,d)). Finally, was compared 1–5 and 1–2 samples and shows an increase in particle size. In the other hand, high concentration of reactants increased agglomeration, and thus led to increase particles size (Figure 10(b,e)). Table 5 shows the average diameter of particles shown by SEM of the prepared samples. The best conditions for getting a small sized and less agglomerated nanostructure materials for this CPC are temperature, reaction time, the power of ultrasonic irradiation and concentration of reactants 30 °C, 60 min, 60 W, and 0.05 M, respectively. Also, other condition (temperature = 60°C, reaction time= 30 min, power of ultrasonic irradiation = 60W and concentration of reactants= 0.05 M) is good for obtaining small nanoparticle size.

IR spectra of compound **1** shows the characteristic stretching frequency of H_2O group observed at around 3474 cm^{-1}, relatively weak absorption bands centered on 3000 cm^{-1} assigned to the C–H stretching frequency of the aromatic rings. The absorption bands with variable intensity in the frequency range between 1700 and 1750 cm^{-1} correspond to C=O stretching frequency of the carbonyl from the 2-pyridinecarboxylic acid ligand. Also, the characteristic band of the C–O stretching frequency carboxylic acid group appeared between 1000 and 1300 cm^{-1}. For the SCN ligand, a stretching band around 2050 cm^{-1} was assigned to SCN group. In addition, two bands around 1500–1700 cm^{-1} revealed the presence of C=C stretching frequency corresponding to the amine group of the ligand (Figure 11).

The TG curve of compound **1** indicates that the compound does melt and is stable up to 80 °C at that temperature it begins to decompose (Figure 8). A first weight loss over 50–100 °C corresponding to the loss of lattice water molecules. The decomposition of coordinated water (mass

loss of 8.7%), pyridine aromatic ring, carboxylate groups of 2-pyridinecarboxylic acid ligand and isothiocyanate groups (mass loss of them 77.4%), occur in range of 110–470 °C. Mass loss calculations show that the final decomposition product is Cu (Figure 19).

Conclusion

One Cu(II) CPC $[Cu(L)(SCN)(H_2O)_2]_n.2H_2O$ (**1**), L=picolinic acid ligand, has been synthesized utilizing a thermal gradient approach and also by sonochemical irradiation. Compound **1** was structurally characterized by single crystal X-ray diffraction. The crystal structure of compound **1** is made up of 1D CPC and shows that the coordination number of Cu (II) ion in compound **1** is six. Also, topology, Hirshfeld surface analyses and thermal behavior were studied for **1**. Influences of temperature, power ultrasound, reaction time and concentration of reactants on the morphological properties of $[Cu(L)(SCN)(H_2O)_2]_n.2H_2O$ (**1**), was studied. The results showed that higher temperature of reagents led to decrease in particle size and optimum time for the process was obtained 60 min, increasing in the power of ultrasonic irradiation led to decrease particles size and high concentration of reactants increased agglomeration, and thus led to increase particles size for **1**. Also, the best conditions for getting a small sized and less agglomerated nanostructure material for this coordination compounds are temperature, reaction time, the power of ultrasonic irradiation and concentration of reactants are 30 °C, 60 min 60 W, and 0.05 M, respectively. These results demonstrated that the use of ultrasounds and the correct selection of different parameters can led to the formation of expected morphologies then the project can be defined more clearly.

Supplementary information

Crystallographic data for the structure reported in this paper have been deposited with the Cambridge Crystallographic Data Center as supplementary publication no. CCDC-1552099. Copies of the data can be obtained upon application to CCDC, 12 Union Road, Cambridge CB2 1EZ, UK (Fax: +44 1223/336033; e-mail: deposit@ccdc.cam.ac.uk).

Acknowledgment

Support of this investigation by University of Sistan and Baluchestan (USB) is gratefully acknowledged. Payam Hayati would like to thanks Professor Davide.M.Proserpio (Milan, Italy) for teaching ToposPro lessons and Eugeny V. Alexandrov (Samara, Russia) for many fruitful discussions about coordination compounds topology.

References

[1] Beloglazkina, E.; Majouga, A.; Moiseeva, A.; Yudin, L.; Moiseev, F.; Shmatova, O.; Zyk, N. Synthesis and Electrochemical Characterization of Complexes of 1, 2-bis [2-(pyridylmethylideneamino) phenylthio] Ethanes with Transition Metals (CoII, NiII, CuII). *Russ. Chem. Bull.* **2008**, *57*, 358–363. DOI: 10.1007/s11172-008-0055-2.

[2] Morshedi, M.; Amirnasr, M.; Triki, S.; Khalaji, A. D. New $(NS)_2$ Schiff Base with a Flexible Spacer: Synthesis and Structural Characterization of Its First Coordination Polymer $[Cu_2(\mu\text{-}I)_2(\mu\text{-}(thio)_2dapte)]_n$ (1). *Inorg. Chim. Acta* **2009**, *362*, 1637–1640. DOI: 10.1016/j.ica.2008.07.002.

[3] Song, Y. J.; Kwak, H.; Lee, Y. M.; Kim, S. H.; Lee, S. H.; Park, B. K.; Jun, J. Y.; Yu, S. M.; Kim, C.; Kim, S.-J.; Kim, Y. Metal-Directed Supramolecular Assembly of Metal (II) Benzoates (M=Co, Ni, Cu, Zn, Mn, and Cd) with 4, 4′-Bipyridine: Effects of Metal Coordination Modes and Novel Catalytic Activities. *Polyhedron* **2009**, *28*, 1241–1252. DOI: 10.1016/j.poly.2009.02.014.

[4] Du, M.; Zhao, X.-J. $\{[Cu(Bipy)_{2.5}(H_2O)](ClO_4)_2\cdot(H_2O)\cdot(CH_3OH)_{1.5}\}_n$ (Bipy = 4, 4′-bipyridine): Organic Template Effect in Formation of a Novel Bilayer Coordination Polymer with Large Chiral Channels. *Inorg. Chem. Commun.* **2004**, *7*, 1056–1060. DOI: 10.1016/j.inoche.2004.07.020.

[5] Huang, F.-P.; Tian, J.-L.; Gu, W.; Yan, S.-P. Three 3D Cu(II) Coordination Polymers Constructed from 1, 2, 4, 5-Benzenetetracarboxylate Acid and Three Positional Isomeric Ligands. *Inorg. Chem. Commun.* **2010**, *13*, 90–94. DOI: 10.1016/j.inoche.2009.10.025.

[6] Kim, S. H.; Park, B. K.; Song, Y. J.; Yu, S. M.; Koo, H. G.; Kim, E. Y.; Poong, J. L; Lee, J. H.; Kim, C.; Kim, S.-J.; Kim, Y. Construction of Crystal Structures of Metal (II)–Benzoates (M=Mn, Ni, Co, Cu, Zn, and Cd) and 1, 2-bis (4-pyridyl) Ethane: Effects of Metal Coordination Modes and Their Catalytic Activities. *Inorg. Chim. Acta* **2009**, *362*, 4119–4126. DOI: 10.1016/j.ica.2009.06.008.

[7] Xu, L.; Wang, E.; Peng, J.; Huang, R. A Novel Coordination Polymer with Double Chains Structure: Hydrothermal Syntheses, Structures and Magnetic Properties of $[Cu(Phen)(H_2O)_2SO_4]_n$ (Phen = 1, 10-phenanthroline). *Inorg. Chem. Commun.* **2003**, *6*, 740–743. DOI: 10.1016/S1387-7003(03)00055-8.

[8] Gao, L.; Zhao, B.; Li, G.; Shi, Z.; Feng, S. Mixed Solvothermal Synthesis and X-ray Characterization of a Layered Copper Coordination Polymer, $Cu(H_2O)(1, 3\text{-}BDC)\cdot H_2O$ (BDC=benzenedicarboxylate). *Inorg. Chem. Commun.* **2003**, *6*, 1249–1251. DOI: 10.1016/S1387-7003(03)00242-9.

[9] Jin, S.-W.; Chen, W.-Z. Synthesis and Characterization of Cu(II), Co(II) and Ni(II) Coordination Polymers Containing bis (imidazolyl) Ligands. *Polyhedron* **2007**, *26*, 3074–3084. DOI: 10.1016/j.poly.2007.02.029.

[10] Goforth, A. M.; Gerth, K.; Smith, M. D.; Shotwell, S.; Bunz, U. H.; Zur Loye, H.-C. Channel-Containing Structures Generated from Linear Coordination Polymer Chains Containing N, N′-Bidentate Ligands and Cu–Cu Dimetal Units. *Solid State Sci.* **2005**, *7*, 1083–1095. DOI: 10.1016/j.solidstatesciences.2005.03.006.

[11] Xiong, K.; Jiang, F.; Gai, Y.; Yuan, D.; Chen, L.; Wu, M.; Su, K.; Hong, M. Truncated Octahedral Coordination Cage Incorporating Six Tetranuclear-Metal Building Blocks and Twelve Linear Edges. *Chem. Sci.* **2012**, *3*, 2321–2325. DOI: 10.1039/c2sc20264f.

[12] Zhang, H.; Pu, W.; Xiong, T.; Li, Y.; Zhou, X.; Sun, K.; Liu, Q.; Zhang, Q. Copper-Catalyzed Intermolecular Aminocyanation and Diamination Of Alkenes. *Angew. Chem. Int. Ed.* **2013**, *52*, 2529–2533. DOI: 10.1002/anie.201209142.

[13] Zhang, L.; Bi, X.; Guan, X.; Li, X.; Liu, Q.; Barry, B. D.; Liao, P. Chemoselective Oxidative C (CO)-C (methyl) Bond Cleavage of Methyl Ketones to Aldehydes Catalyzed by CuI with Molecular Oxygen. *Angew. Chem.* **2013**, *125*, 11513–11517. DOI: 10.1002/ange.201305010.

[14] Dhayal, R. S.; Liao, J.-H.; Lin, Y.-R.; Liao, P.-K.; Kahlal, S.; Saillard, J.-Y.; Liu, C. A Nanospheric Polyhydrido Copper Cluster of Elongated Triangular Orthobicupola Array: Liberation of H_2 from Solar Energy. *J. Am. Chem. Soc.* **2013**, *135*, 4704–4707. DOI: 10.1021/ja401576s.

[15] Khnayzer, R. S.; McCusker, C. E.; Olaiya, B. S.; Castellano, F. N. Robust Cuprous Phenanthroline Sensitizer for Solar Hydrogen Photocatalysis. *J. Am. Chem. Soc.* **2013**, *135*, 14068–14070. DOI: 10.1021/ja407816f.

[16] Liu, K.; Sun, Y.; Deng, L.; Cao, F.; Han, J.; Wang, L. Cu(II) Coordination Polymers Constructed by Tetrafluoroterephthalic Acid and Varied Imidazole-Containing Ligands: Syntheses, Structures and Properties. *J. Solid State Chem.* **2018**, *258*, 24–31. DOI: 10.1016/j.jssc.2017.10.002.

[17] Liu, K.; Deng, L.; Zhang, Y.; Jiao, S.; Geng, Y.; Wang, L. Coordination Behavior of bis-Imidazole and Various Carboxylate Ligands Towards Zn(II) and Cd(II) ions: Synthesis, Structure, and Photoluminescence Study. *Crystals* **2018**, *8*, 236. DOI: 10.3390/cryst8060236.

[18] Liu, K.; Hu, H.; Sun, J.; Zhang, Y.; Han, J.; Wang, L. pH–Value-Controlled Assembly of Photoluminescent Zinc Coordination Polymers in the Mixed-Ligand System. *J. Mol. Struct.* **2017**, *1134*, 174–179. DOI: 10.1016/j.molstruc.2016.12.075.

[19] Kawaguchi, S. Variety in the Coordination Modes of *β*-Dicarbonyl Compounds in Metal Complexes. *Coordinat. Chem. Rev.* **1986**, *70*, 51–84. DOI: 10.1016/0010-8545(86)80035-2.

[20] Shan, Z.; Stach, E.; Wiezorek, J.; Knapp, J.; Follstaedt, D.; Mao, S. Grain Boundary-Mediated Plasticity in Nanocrystalline Nickel. *Science* **2004**, *305*, 654–657. DOI: 10.1126/science.1098741.

[21] Fard, M. J. S.; Hayati, P.; Naraghi, H. S.; Tabeie, S. A. Synthesis and Characterization of a New Nano Lead (II) 0-D Coordination Supramolecular Compound: A Precursor to Produce Pure Phase Nano-Sized Lead (II) Oxide. *Ultrason. Sonochem.* **2017**, *39*, 129. DOI: 10.1016/j.ultsonch.2017.04.023.

[22] Fard, M. J. S.; Hayati, P.; Firoozadeh, A.; Janczak, J. Ultrasonic Synthesis of Two New Zinc (II) Bipyridine Coordination Polymers: New Precursors for Preparation Of Zinc (II) Oxide Nano-Particles. *Ultrason. Sonochem.* **2017**, *35*, 502–513. DOI: 10.1016/j.ultsonch.2016.11.009.

[23] Akhbari, K.; Morsali, A.; Retailleau, P. Effect Of Two Sonochemical Procedures on Achieving to Different Morphologies of Lead(II) Coordination Polymer Nano-Structures. *Ultrason. Sonochem.* **2013**, *20*, 1428–1435. DOI: 10.1016/j.ultsonch.2013.03.013.

[24] Fard, M. J. S.; Hayati, P.; Firoozadeh, A.; Janczak, J. Sonochemical Synthesis of Two New Zinc(II) 1, 10-Phenanthroline Coordination Supramolecular Compounds: New Precursors to Produce Nano-Sized Zinc (II) Oxide. *Ultrason. Sonochem.* **2017**, *37*, 286–297. DOI: 10.1016/j.ultsonch.2017.01.020.

[25] Abbasi, A. R.; Morsali, A. Influence of Solvents on the Morphological Properties of AgBr Nano-Structures Prepared Using Ultrasound Irradiation. *Ultrason. Sonochem.* **2012**, *19*, 540–554. DOI: 10.1016/j.ultsonch.2011.08.002.

[26] Goher, M. A. S.; Abu-Youssef, M. A. M.; Mautner, F. A. Crystal Structure Investigation of Copper(II) Thiocyanato and Cobalt (III Azido Complexes of Picolinic Acid; [Cu (Pic)(SCN)$(H_2O)_2$]·$2H_2O$ and [Na_2Co(Pic)$_2$$(N_3)_2$$(H_2O)_6$][Co (Pic)$_2$$(N_3)_2$]·$2H_2O$. *Zeitschrift Für Naturforschung B* **1993**, *48*, 1795–1800. DOI: 10.1515/znb-1993-1216.

[27] Cao, S.; Jiang, J.; Zhu, B.; Yu, J. Shape-Dependent Photocatalytic Hydrogen Evolution Activity Over a Pt Nanoparticle Coupled gC_3N_4 Photocatalyst. *Phys. Chem. Chem. Phys.* **2016**, *18*, 19457–19463. DOI: 10.1039/C6CP02832B.

[28] Khan, I.; Ali, S.; Mansha, M.; Qurashi, A. Sonochemical Assisted Hydrothermal Synthesis of Pseudo-Flower Shaped Bismuth Vanadate ($BiVO_4$) and Their Solar-Driven Water Splitting Application. *Ultrason. Sonochem.* **2017**, *36*, 386–392. DOI: 10.1016/j.ultsonch.2016.12.014.

[29] Bang, J. H.; Suslick, K. S. Applications of Ultrasound to the Synthesis of Nanostructured Materials. *Adv. Mater.* **2010**, *22*, 1039–1059. DOI: 10.1002/adma.200904093.

[30] Okitsu, K.; Ashokkumar, M.; Grieser, F. Sonochemical Synthesis of Gold Nanoparticles: Effects Of Ultrasound Frequency. *J. Phys. Chem. B* **2005**, *109*, 20673–20675. DOI: 10.1021/jp0549374.

[31] Siedl, N.; Baumann, S. O.; Elser, M. J.; Diwald, O. Particle Networks from Powder Mixtures: Generation of TiO_2–SnO_2 Heterojunctions Via Surface Charge-Induced Heteroaggregation. *J. Phys. Chem. C* **2012**, *116*, 22967–22973. DOI: 10.1021/jp307737s.

[32] da Silva, G. T.; Carvalho, K. T.; Lopes, O. F.; Ribeiro, C. gC_3N_4/Nb_2O_5 Heterostructures Tailored by Sonochemical Synthesis: Enhanced Photocatalytic Performance in Oxidation of Emerging Pollutants Driven by Visible Radiation. *App. Catal. B Environ.* **2017**, 216, 70–79. DOI: 10.1016/j.apcatb.2017.05.038.

[33] Koch, C. C. Ductility in Nanostructured and Ultra Fine-Grained Materials: Recent Evidence for optimism. *Jmnm.* **2003**, *18*, 9–20. DOI: 10.4028/www.scientific.net/JMNM.18.9.

[34] Jun, Y-w.; Seo, J-w.; Oh, S. J.; Cheon, J. Recent Advances in the Shape Control Of Inorganic Nano-Building Blocks. *Coordinat. Chem. Rev.* **2005**, *249*, 1766–1775. DOI: 10.1016/j.ccr.2004.12.008.

[35] Shi, H.; Qi, L.; Ma, J.; Cheng, H. Polymer-Directed Synthesis of Penniform BaWO4 Nanostructures in Reverse Micelles. *J. Am. Chem. Soc.* **2003**, *125*, 3450–3451. DOI: 10.1021/ja029958f.

[36] Kim, J. H.; Andeen, D.; Lange, F. F. Hydrothermal Growth of Periodic, Single-Crystal ZnO Microrods and Microtunnels. *Adv. Mater.* **2006**, *18*, 2453–2457. DOI: 10.1002/adma.200600257.

[37] Kuang, D.; Xu, A.; Fang, Y.; Liu, H.; Frommen, C.; Fenske, D. Surfactant-Assisted Growth of Novel PbS Dendritic Nanostructures Via Facile Hydrothermal Process. *Adv. Mater.* **2003**, *15*, 1747–1750. DOI: 10.1002/adma.200304623.

[38] Kim, F.; Connor, S.; Song, H.; Kuykendall, T.; Yang, P. Platonic Gold Nanocrystals. *Angew. Chem.* **2004**, *116*, 3759–3763. DOI: 10.1002/ange.200454216.

[39] Lv, S.; Li, P.; Sheng, J.; Sun, W. Synthesis of Single-Crystalline $BaCO_3$ Nanostructures with Different Morphologies via a Simple PVP-Assisted Method. *Mater. Lett.* **2007**, *61*, 4250–4254. DOI: 10.1016/j.matlet.2007.01.075.

[40] Hayati, P.; Rezvani, A. R.; Morsali, A.; Retailleau, P.; García-Granda, S. Influences of Temperature, Power Ultrasound and Reaction Time on the Morphological Properties of Two New Mercury (II) Coordination Supramolecular Compounds. *Ultrason. Sonochem.* **2017**, *34*, 968–977. DOI: 10.1016/j.ultsonch.2016.07.019.

[40] Hayati, P.; Rezvani, A. R.; Morsali, A.; Retailleau, P.; García-Granda, S. Influences of Temperature, Power Ultrasound and Reaction Time on the Morphological Properties of Two New Mercury (II) Coordination Supramolecular Compounds. *Ultrason. Sonochem.* **2017**, *34*, 968–977. DOI: 10.1016/j.ultsonch.2016.07.019.

[40] Hayati, P.; Rezvani, A. R.; Morsali, A.; Retailleau, P.; García-Granda, S. Influences of Temperature, Power Ultrasound and Reaction Time on the Morphological Properties of Two New Mercury (II) Coordination Supramolecular Compounds. *Ultrason. Sonochem.* **2017**, *34*, 968–977. DOI: 10.1016/j.ultsonch.2016.07.019.

[41] Hayati, P.; Rezvani, A.; Morsali, A.; Retailleau, P.; Centore, R. Survey of Temperature, Reaction Time and Ultrasound Irradiation Power on Sonochemical Synthesis of Two New Nanostructured Lead (II) Coordination Supramolecule Compounds. *Ultrason. Sonochem.* **2017**, *35*, 81–91. DOI: 10.1016/j.ultsonch.2016.09.005.

[42] Abbasi, A. R.; Morsali, A. Syntheses and Characterization of AgI Nano-Structures by Ultrasonic Method: different Morphologies under Different Conditions. *Ultrason. Sonochem.* **2010**, *17*, 572–578. DOI: 10.1016/j.ultsonch.2009.11.002.

[43] Abbasi, A. R.; Morsali, A. Formation of Silver Iodide nanoparticles on silk Fiber by Means of Ultrasonic Irradiation. *Ultrason. Sonochem.* **2010**, *17*, 704–710. DOI: 10.1016/j.ultsonch.2010.01.002.

[44] Hayati, P.; Rezvani, A. R.; Morsali, A.; Retailleau, P. Ultrasound Irradiation Effect on Morphology and Size of Two New Potassium

Coordination Supramolecule Compounds. *Ultrason. Sonochem.* **2017**, *34*, 195–205. DOI: 10.1016/j.ultsonch.2016.05.031.

[45] Hayati, P.; Rezvani, A. R.; Morsali, A.; Molina, D. R.; Geravand, S.; Suarez-Garcia, S.; Villaecija, M. A. M.; García-Granda, S.; Mendoza-Meroño, R.; Retailleau, P. Sonochemical Synthesis, Characterization, and Effects of Temperature, Power Ultrasound and Reaction Time on the Morphological Properties of Two New Nanostructured Mercury(II) Coordination Supramolecule Compounds. *Ultrason. Sonochem.* **2017**, *37*, 382–393. DOI: 10.1016/j.ultsonch.2017.01.021.

[46] Hou, L.; Li, D.; Shi, W.-J.; Yin, Y.-G.; Ng, S. W. Ligand-Controlled Mixed-Valence Copper Rectangular Grid-Type Coordination Polymers Based on Pyridylterpyridine. *Inorg. Chem.* **2005**, *44*, 7825–7832. DOI: 10.1021/ic050558d.

[47] Chen, G.; Bai, Z. P.; Qu, S. J. Catena-Poly [[dipyridylcopper (II)]-di-μ-thiocyanato]. *Acta Crystallograph.* **2005**, *61*, m2718–m2719.

[48] Wang, B.-Y.; Xu, W.-J.; Xue, W.; Lin, R.-B.; Du, Z.-Y.; Zhou, D.-D.; Zhang, W.-X.; Chen, X.-M. Restraining the Motion of a Ligand for Modulating the Structural Phase Transition in Two Isomorphic Polar Coordination Polymers. *Dalton Trans.* **2014**, *43*, 9008–9011. DOI: 10.1039/C4DT00675E.

[49] Vančo, J.; Trávníček, Z.; Marek, J.; Herchel, R. Synthesis, Spectral (UV–Vis, IR, ESI-MS), Magnetic and Structural Characterizations, and the Antimicrobial Effect of Potassium Isothiocyanato-(N-Salicylidene-Amino-Acidato) Cuprates. *Inorg. Chim. Acta* **2010**, *363*, 3887–3896. DOI: 10.1016/j.ica.2010.07.041.

[50] Rigaku. *CrystalClear-SM Expert 2.1b43*. Rigaku Corporation: Tokyo, Japan, **2014**.

[51] Sheldrick, G. M. SHELXT: Integrating space group determination and structure solution. *Acta Crystallogr., Sect. A: Found. Adv* .70 , 2014: C1437

[52] Spek, A. L. Structure validation in chemical crystallography. *Acta Crystallogr. D Biol. Crystallogr.* **2009**, *D65*, 148–155. DOI: 10.1107/S090744490804362X.

[53] *SADABS*, Bruker-Nonius: Delft, The Netherlands, **2002**.

[54] A.; Altomare, M. C.; Burla, M.; Camalli, G. L.; Cascarano, C.; Giacovazzo, A.; Guagliardi, G. G.; Moliterni, G.; Polidori, R.; Spagna, J. SIR 97: A New Tool for Crystal Structure Determination and Refinement. *J. Appl. Crystallogr.* **1999**, *32*, 115–119. DOI: 10.1107/S0021889898007717.

[55] Sheldrick, G. M. A Short History of SHELX. *Acta Crystallogr., A, Found. Crystallogr* **2008**, *64*, 112–122. DOI: 10.1107/S0108767307043930.

[56] Farrugia, L. J. WinGX and ORTEP for Windows : An Update. *J. Appl. Crystallogr.* **2012**, *45*, 849–854. DOI: 10.1107/S0021889812029111.

[57] Mercury 1.4.1, Copyright Cambridge Crystallographic Data Centre, 12 Union Road, Cambridge, CB2 1EZ, UK, 2001–2005.

[58] Dolomanov, O. V.; Bourhis, L. J.; Gildea, R. J.; Howard, J. A.; Puschmann, H. OLEX2: A Complete Structure Solution, Refinement and Analysis Program. *J. Appl. Crystallogr.* **2009**, *42*, 339–341. DOI: 10.1107/S0021889808042726.

[59] Suslick, K. S. Sonochemistry. *Science* **1990**, *247*, 1439–1445. DOI: 10.1126/science.247.4949.1439.

[60] Suslick, K. S.; Flannigan, D. J. Inside a Collapsing Bubble: sonoluminescence and the Conditions during Cavitation. *Annu. Rev. Phys. Chem.* **2008**, *59*, 659–683. DOI: 10.1146/annurev.physchem.59.032607.093739.

[61] Blatov, V. A.; Shevchenko, A. P.; Proserpio, D. M. Applied Topological Analysis of Crystal Structures with the Program Package ToposPro. *Crystal Growth Design* **2014**, *14*, 3576–3586. http://topospro.com. DOI: 10.1021/cg500498k.

[62] Alexandrov, E. V.; Blatov, V. A.; Kochetkov, A. V.; Proserpio, D. M. Underlying Nets in Three-Periodic Coordination Polymers: topology, Taxonomy and Prediction from a Computer-Aided Analysis of the Cambridge Structural Database. *CrystEngComm* **2011**, *13*, 3947–3958. DOI: 10.1039/c0ce00636j.

[63] CnesnN, E.; Worne, N. C. Crystal Habit of Synthetic Ghalcanthite (Copper Sulfate Pentahydrate) as Related to Position and Orientation in Growth Solution. *Am. Mineral* **1974**, *59*, 1105–1112.

[64] Urgut, O.; Ozturk, L; Banti, C.; Kourkoumelis, N.; Manoli, M.; Tasiopoulos, A.; Hadjikakou, S. New Antimony(III) Halide Complexes with Dithiocarbamate Ligands Derived from Thiuram Degradation: The Effect of the Molecule's Close Contacts on in Vitro Cytotoxic Activity. *Mater. Sci. Eng. C* **2016**, *58*, 396–408. DOI: 10.1016/j.msec.2015.08.030.

[65] Urgut, O.; Ozturk, L; Banti, C.; Kourkoumelis, N.; Manoli, M.; Tasiopoulos, A.; Hadjikakou, S. Addition of Tetraethylthiuram Disulfide to Antimony (III) Iodide; Synthesis, Characterization and Biological Activity. *Inorg. Chim. Acta* **2016**, *443*, 141–150. DOI: 10.1016/j.ica.2015.12.028.

[66] Spackman, M. A.; McKinnon, J. J. Fingerprinting Intermolecular Interactions in Molecular Crystals. *CrystEngComm* **2002**, *4*, 378–392. DOI: 10.1039/B203191B.

[67] Bouaziz, E.; Hassen, C. B.; Chniba-Boudjada, N.; Daoud, A.; Mhiri, T.; Boujelbene, M. Crystal Structure, Hirshfeld Surface Analysis, Vibrational, Thermal Behavior and UV Spectroscopy of (2, 6-Diaminopyridinium) Dihydrogen Arsenate. *J. Mol. Struct.* **2017**, *1145*, 121. DOI: 10.1016/j.molstruc.2017.05.043.

[68] Jayatilaka, D.; McKinnon, J.; Spackman, M. Towards Quantitative Analysis of Intermolecular Interactions with Hirshfeld Surfaces. *Chem. Commun.* **2007**, *37*, 3814. DOI: 10.1039/b704980c.

[69] Spackman, M. A.; Jayatilaka, D. Hirshfeld Surface Analysis. *CrystEngComm* **2009**, *11*, 19–32. DOI: 10.1039/B818330A.

[70] Bitzer, R. S.; Visentin, L. C.; Hörner, M.; Nascimento, M. A. C.; Filgueiras, C. A. L. On the Molecular and Supramolecular Properties of N, N′-Disubstituted Iminoisoindolines: Synthesis, Spectroscopy, X-Ray Structure and Hirshfeld Surface Analyses, and DFT Calculations of Two (E)-N, N′-Bis(Aryl)Iminoisoindolines (Aryl = 2-Tert-Butylphenyl or Perfluorophenyl). *J. Mol. Struct* **2017**, *1130*, 165. DOI: 10.1016/j.molstruc.2016.10.029.

[71] Majumdar, D.; Biswas, J. K.; Mondal, M.; Babu, M. S.; Metre, R. K.; Das, S.; Bankura, K.; Mishra, D. Coordination of N, O-Donor Appended Schiff Base Ligand (H_2L_1) towards Zinc(II) in Presence of Pseudohalides: Syntheses, Crystal Structures, Photoluminescence, Antimicrobial Activities and Hirshfeld Surfaces. *J. Mol. Struct.* **2018**, *1155*, 745–757. DOI: 10.1016/j.molstruc.2017.11.052.

[72] Majumdar, D.; Dey, S.; Sreejith, S. S.; Biswas, J. K.; Mondal, M.; Shukla, P.; Das, S.; Pal, T.; Das, D.; Bankura, K.; Mishra, D. Syntheses, Crystal Structures and Photo Physical Aspects of Azido-Bridged Tetranuclear Cadmium(II) Complexes: DFT/TD-DFT, Thermal, Antibacterial and anti-Biofilm Properties. *J. Mol. Struct.* **2019**, *1179*, 694–708. DOI: 10.1016/j.molstruc.2018.11.010.

[73] Majumdar, D. J.; Dey, S.; Sreekumar, S. S.; Das, S.; Das, D.; Metre, R. K.; Bankura, K.; Mishra, D. Nitrato, Pseudohalo-Linked Zn(II)/Cd(II) Schiff-Base Complexes with 1, 3-Diimine Spacer Group: Syntheses, Crystal Structures, DFT, TD-DFT and Fluorescence Studies. *Chem. Select* **2018**, *3*, 12371–12382. DOI: 10.1002/slct.201802996.

[74] Goher, M. A. S.; Abu-Youssef, M. A. M.; Mautner, F. A. Crystal Structure Investigation of Copper(II) Thiocyanato and Cobalt (III Azido Complexes of Picolinic Acid; [Cu (Pic)(SCN)(H2O)2]· 2H2O and [Na2Co(Pic)2(N3)2(H2O)6][Co (Pic)2(N3)2]· 2H2O. *Zeitschrift Für Naturforschung B* **1993**, *48*, 1795–1800.

[75] Daković, M.; Jagličić, Z.; Kozlevčar, B.; Popović, Z. Association of Copper(II) Isonicotinamide Moieties via Different Anionic Bridging Ligands: Two Paths of Ferromagnetic Interaction in the Azide Coordination Compound. *Polyhedron* **2010**, *29*, 1910–1917. DOI: 10.1016/j.poly.2010.02.040.

[76] Das, L. K.; Diaz, C.; Ghosh, A. Antiferromagnetic Mixed-Valence Cu(I)–Cu(II) Two-Dimensional Coordination Polymers

Constructed by Double Oximato Bridged Cu(II) Dimers and CuISCN Based One-Dimensional Anionic Chains. *Crystal Growth Design* **2015**, *15*, 3939–3949. DOI: 10.1021/acs.cgd.5b00560.

[77] Kabešová, M.; Dunaj-Jurčo, M.; Soldanova, J. Crystal and Molecular Structure of Bis (4-Bromopyridine) Dithiocyanate Copper(II). *Inorg. Chim. Acta* **1987**, *130*, 105–111. DOI: 10.1016/S0020-1693(00)85937-X.

[78] Koziskova, Z.; Kozisek, J.; Kabesova, M. Three Different Copper(II) Coordination Polyhedra in the Crystal Structure of Bis (4-Picoline) Dithiocyanato Copper(II) Complex,$[Cu(4\text{-}Pic)_2(NCS)_2]$; Experimental Evidence of a New Type of Mutual Influence of Ligands in Complexes. *Polyhedron* **1990**, *9*, 1029–1034.

[79] Małecki, J.; Machura, B.; Świtlicka, A.; Kusz, J. X-Ray Studies, Spectroscopic Characterization and DFT Calculations for Mn(II), Ni(II) and Cu(II) Complexes with 2-Benzoylpyridine. *Polyhedron* **2011**, *30*, 410–418. DOI: 10.1016/j.poly.2010.11.013.

[80] Wriedt, M.; Näther, C. In Situ Solid State Formation of Copper(I) coordination Polymers by Thermal Reduction of Copper(II) Precursor Compounds: structure and Reactivity of $[Cu(NCS)_2 \ (Pyrimidine)_2]_\infty$. *Dalton Trans.* **2009**, *46*,10192–10198. DOI: 10.1039/b909838k.

[81] Čobeljić, B.; Pevec, A.; Turel, I.; Spasojević, V.; Milčić, M.; Mitić, D.; Sladić, D.; Anđelković, K. Analysis of the Structures of the Cu(I) and Cu(II) Complexes with 3-Acetylpyridine and Thiocyanate. *Polyhedron* **2014**, *69*, 77–83. DOI: 10.1016/j.poly.2013.11.027.

[82] Karadag, A.; Yilmaz, V. T.; Thoene, C. Di-and Triethanolamine Complexes of Co(II), Ni(II), Cu(II) and Zn(II) with Thiocyanate: synthesis, Spectral and Thermal Studies. Crystal Structure of Dimeric Cu (II) Complex with Deprotonated Diethanolamine,$[Cu_2(\mu\text{-Dea})_2(NCS)_2]$. *Polyhedron* **2001**, *20*, 635–641. DOI: 10.1016/S0277-5387(01)00720-3.

[83] Mikuriya, M.; Kida, S.; Murase, I. Preparation and Crystal Structures of Binuclear Copper(II) Complexes of N, N′, N″, N‴-Tetrakis (2-Aminoethyl) 1, 4, 8, 11-Tetraazacyclotetradecane Containing Azide, Cyanate, or Thiocyanate Ion. *Bcsj.* **1987**, *60*, 1355–1359. DOI: 10.1246/bcsj.60.1355.

[84] Machura, B.; Świtlicka, A.; Mroziński, J.; Kalińska, B.; Kruszynski, R. Structural Diversity and Magnetic Properties of Thiocyanate Copper(II) Complexes. *Polyhedron* **2013**, *52*, 1276–1286. DOI: 10.1016/j.poly.2012.06.019.

[85] Domínguez, S.; Torres, J.; González-Platas, J.; Hummert, M.; Schumann‖, H.; Kremer, C. Thermodynamic Stability and Crystal Structure of Lanthanide Complexes with di-2-Pyridyl Ketone. *J. Coordinat. Chem.* **2009**, *62*, 108–119. DOI: 10.1080/00958970802474797.